Predicting and optimizing the energy-generation performance of an in-stream turbine operating with twin, unconfined, counter-rotating screws by means of CFD Modeling

Alexandre Lamoureux, Duane J. M. Baker, Jean Doyon, and Ross Sinclaire

Abstract—**The overall objective of this numerical investigation consists of predicting and optimizing the energy-generation performance of an in-stream turbine undergoing preliminary design. This turbine is unconventional as its energy extraction surfaces are composed of twin, counter-rotating, unconfined screws aligned at an oblique angle with respect to the water current. First, a cost-effective computational fluid dynamics (CFD) model of the water flow in the vicinity of the turbine was implemented in a commercial package. This CFD model was benchmarked by comparing predicted power coefficient values with available, empirically-obtained, data provided by the client. During this benchmarking exercise, it was determined that a rotating (sliding) mesh approach was necessary to obtain accurate predictions. The CFD model was then used to predict power coefficient values over a range of tip-speed ratios at the design free-stream water velocity for the proposed (initial) screw design. Lastly, simulations were performed to investigate the performance of additional screw designs in the hope of optimizing the energy-generation performance while respecting the provided design constraints.**

Keywords—**Computational fluid dynamics modeling, in-stream turbine, hydrokinetic turbine, renewable energy, performance optimization.**

I. Introduction

HYDROKINETIC or in-stream turbines have been receiving increasing attention over the last decades. These devices are typically designed with the aim of converting the kinetic energy available in river streams and tidal currents into electricity. Under certain circumstances, in-stream turbines can be viewed as a preferable alternative to conventional types of power generation including hydropower. Examples of such circumstances include the following: i) depending on the retained criteria, in-stream turbines could offer a reduced environmental footprint, ii) they are likely to require fewer capital expenditures for small-scale production, iii) they allow progressive and incremental implementation, and iv) they can be considered as being mobile to some extent (allowing installation, removal and relocation with reasonable effort). For specific applications, such as small-scale remote power generation, they could prove to be the sole viable option based on renewable energy.

Most in-stream turbine designs fall under one of the following three categories: i) horizontal axis, ii) cross flow, and iii) vertical axis. Reviews of existing designs, their respective advantages and drawbacks, operating challenges and environmental impacts can be found in the works of Khan *et al.* [1], Güney and Kaygusuz [2], Yuce and Muratoglu [3], Khan *et al.* [4] and Aly and El-Hawary [5]. Multiple authors and organisations have also assessed the hydrokinetic power potential of various regions and countries. An example of such an exercise is provided in a report published by the Canadian Hydraulics Centre [6]. Comprehensive reviews of in-stream turbine technologies, hydrokinetic power potential, design considerations, regulations, environmental impacts and effects on waterborne transportation can be found in the works of Ortega-Achury *et al.* [7] and VanZwieten *et al.* [8].

There are ongoing efforts to improve the design of in-stream turbines with the objective to: reduce manufacturing and installation costs, reduce operational costs, increase robustness of design, increase energy-generation performance, reduce impacts on environment and facilitate maintenance, to name a few. Such efforts are often deployed by improving existing and established design configurations. Other attempts include proposing novel or unconventional designs, as was done by a Canadian firm named Jupiter Hydro Inc.

Paper ID number: 1219; Conference track: Tidal hydrodynamic modelling.

A. Lamoureux is with Hatch Ltd., 5 Place Ville Marie, suite 1400, Montreal, Quebec, H3B 2G2, Canada (e-mail: alexandre.lamoureux@hatch.com).

D. J. M. Baker is with Hatch Ltd., 2800 Speakman Dr., Mississauga, Ontario, L5K 2R7, Canada (e-mail: duane.baker@hatch.com).

J. Doyon is with Hatch Ltd., 5 Place Ville Marie, suite 1400, Montreal, Quebec, H3B 2G2, Canada (e-mail: jean.doyon@hatch.com).

R. Sinclaire is with Jupiter Hydro Inc., 2777 Ekers Av., Montreal, Quebec, H3S 1E2, Canada (e-mail: ross.sinclaire@gmail.com).

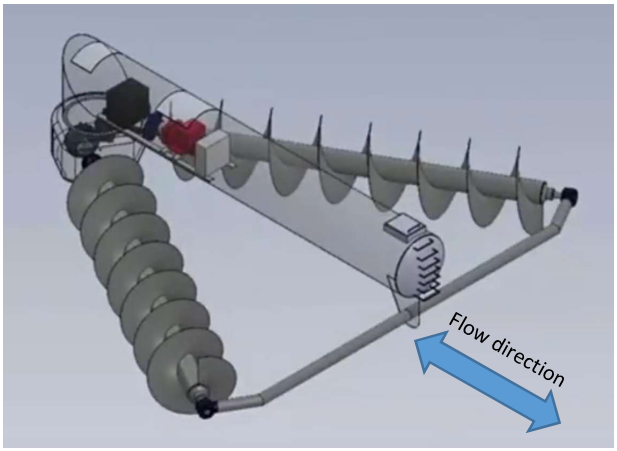

Fig. 1. Schematic of the Jupiter Hydro in-stream turbine (300 kW nominal power variant, 2017 design). Water line not shown. Canadian patent #2,807,876 and US patent #9,279,407 B2.

Jupiter Hydro's in-stream turbine (henceforth referred to as the JH turbine) is undoubtedly unconventional, as its energy extraction surfaces are composed of twin, counter-rotating, unconfined screws aligned at an oblique angle with respect to the water current. A schematic of the JH turbine (300 kW nominal power variant, 2017 design) is shown in Fig. 1.

When submerged and subjected to sufficiently high free stream water velocities, the screws of the turbine rotate and produce a net torque, which is turn transmitted to a generator to produce electricity. The central floating body (hull) contains the equipment required to generate electricity, as well as other systems, such as controls and protections. The rotational speed of the screws is regulated and maintained at the optimal value by the generator which applies the required counter-torque to the screws. Additional design characteristics of this turbine are provided in Section 3.

Jupiter Hydro has approached Hatch Ltd., an engineering and consulting firm, to conduct the preliminary design of the JH turbine (300 kW variant). One of the design activities consisted of optimizing (maximizing) the power-generation performance of the turbine by investigating the performance of various screw designs and dimensions. Computational fluid dynamics (CFD) modeling was chosen and employed as the predictive tool in this exercise. Use of CFD modeling for in-stream turbine design could be considered as an essentially standard and desirable practice in the industry. For examples of recent papers pertaining to numerical modeling of in-stream turbines, the reader is referred to the works of Lawson *et al.* [9], Hall [10], Marsh *et al.* [11] and Neary *et al.* [12].

Numerical investigations of in-stream turbines operating with the aforementioned energy extraction surfaces, namely twin, counter-rotating, unconfined screws aligned at an oblique angle with the flow, have not been found after performing a literature review. Filling this gap is the main motivation of the authors of this article.

It is worth highlighting that there already exist Archimedes' screw turbines operating with partially or fully confined screws having axes aligned along the overall flow direction. Also, they are generally gravity-driven devices and extract energy using distinct flow mechanisms. Consequently, despite their apparent similarity, they are deemed as a different turbine design category by the authors of the present paper.

This article presents the CFD modeling exercise conducted to optimize the power-generation performance of the JH turbine. Focus is put on the challenges associated with accurately modeling the fluid flow over the previously-discussed unconventional energy extraction surfaces. Due to the industrial context and schedule-driven nature of the work, care was taken to implement a cost-effective model which provided sufficiently accurate predictions while maintaining computational efforts (and related costs) under acceptable limits.

II. Objectives of the CFD Modeling Exercise

The detailed objectives of the CFD modeling exercise presented in this paper are listed below, in order of completion:

1) Develop a CFD model implemented in a commercial package allowing for the simulation of the water flow over the energy extraction surfaces (screws) of the JH turbine and yielding accurate predictions of its energy-generation performance at the shafts.
2) Investigate potential model simplifications which can result in significant reductions of computational efforts without adversely affecting the accuracy of the numerical predictions.
3) Benchmark the CFD model predictions, namely power coefficient values over a range of screw tip-speed ratios, with field measurements obtained with an instrumented, smaller scale (1/2) turbine test unit.
4) Use the benchmarked CFD model to predict the performance of the baseline (initial) screw design and investigate the performance of additional, improved screw designs until the key performance criterion, generated power at the shaft, is satisfied and maximized.

The following fifth objective was also part of the CFD modeling exercise but is not discussed in this article, as it lies beyond its scope:

5) Output key simulation results for the chosen (best) screw design, namely instantaneous static pressure fields prevailing over the screw surfaces. These acted as boundary conditions prescribed in a Finite-Element Analysis (FEA) model aimed at investigating the structural integrity of the screws.

TABLE I
DESIGN FEATURES AND CHARACTERISTICS OF THE JH TURBINE (2017 VARIANT, INITIAL DESIGN VALUES)

Symbol	Definition	Value
P_{rated}	Turbine rated power, electrical, at design free stream velocity	300 kW
$V_{\infty,\,design}$	Design water free stream velocity	4 m/s
N_{screws}	Number of screws	2
L_{shaft}	Screw shaft length (bearing to bearing)	12.80 m
D_{screw}	Screw outer membrane diameter	2.29 m
α	Angle between screw axis and hull centreline	30°
H_{screw}	Screw axis immersion depth	2.05 m

III. DESIGN AND CHARACTERISTICS OF MODELED IN-STREAM TURBINE

The key design features and characteristics of the modeled in-stream JH turbine are provided in Table I. It is worth mentioning that the listed values are those of the 2017 variant. Due to confidentiality reasons, some design details, such as screw pitch, screw shaft diameter and number of screw membrane turns, could not be listed.

A schematic of the immersed JH turbine is shown in Fig. 2. Some design features, such as screw outer membrane diameter and screw axis immersion depth, are also depicted in this illustration. The turbine moorings are not shown yet, as they were undergoing design at the time of CFD analysis. Their impact on the water flow field over the screws and the predicted performance of the turbine is assumed to be essentially negligible.

As mentioned earlier, the rotational speed of the screws would be regulated and maintained at the optimal value, thereby maximizing extracted power at the shafts. This optimal rotational speed is not constant and depends on the prevailing free stream water velocity magnitude, V_∞, as can be expected. This rotational speed regulation would be performed by real-time modulation of the generator counter-torque and using embarked instrumentation and control systems. In this preliminary design phase and CFD modeling exercise, attention was put on predicting and maximizing the performance of the turbine in steady-state, or more precisely, in its established time-periodic operation.

The optimal screw rotational speed at which extracted shaft power is maximized (at a certain value of V_∞) is not known first-hand. The approach employed in this study is the following: i) multiple simulations were performed over a range of screw rotational speed values while maintaining the value of $V_{\infty,\,design}$ constant, ii) values of mechanical power produced at the shafts were compiled for each simulated case, iii) results were inspected to determine the maximum mechanical power produced and the corresponding (optimal) screw rotational speed.

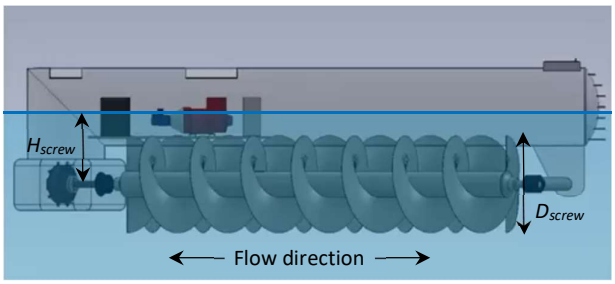

Fig. 2. Schematic showing immersion level of JH turbine. Central hull internal equipment not fully shown for clarity purposes.

This exercise is referred to as developing the power performance curve.

The following well-established dimensionless parameters, namely the power coefficient (C_P) and tip-speed ratio (TSR) are used to present results:

$$C_P = \frac{T\omega}{\frac{1}{2}\rho_w V_\infty^3 A_{proj.}} \tag{1}$$

$$TSR = \frac{(D_{screw}/2)\omega}{V_\infty} \tag{2}$$

In the above-listed equations, T, ω and ρ_w denote respectively: the net torque provided by a single screw, the screw rotational speed (in rad/s) and the mass density of water. Lastly, $A_{proj.}$ represents the projected frontal area of a single screw, defined as follows:

$$A_{proj.} = D_{screw} \times L_{screw} \sin\alpha \tag{3}$$

In (3), L_{screw} is the length of screw shaft over which the screw membrane extends. This value is naturally slightly inferior to L_{shaft}.

IV. NUMERICAL MODELING APPROACH AND METHODOLOGY

This section outlines the approach and methodology followed in this numerical modeling exercise. Boundary conditions and cost-effectiveness considerations are also addressed in this section.

A. Modeling assumptions

The density and dynamic viscosity of water were considered as constant and established values of these properties at 15°C were prescribed in the model.

Inspection of local static pressure values in preliminary simulations indicated that cavitation is not expected to occur near the turbine. Consequently, provisions to predict this phenomenon were not included in the model.

At this preliminary design stage, the turbine was presumed to remain in a fixed and levelled position with respect to the water surface. This is equivalent to assuming infinitely rigid (idealized) mooring. Thus, rigid body motion and attitude changes were not studied as this stage.

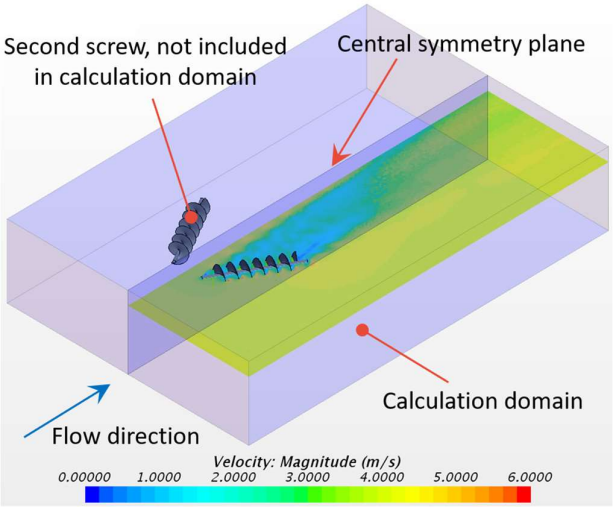

Fig. 3. Schematic of simplified calculation domain (bottom right half only). Sample water velocity magnitude contour plot plotted over horizontal plane coinciding with screw rotation axis, for visualization purposes. Air layer above water volume not shown.

The turbine hull axis was presumed to be exactly aligned with respect to the direction of the water flow. Thus, the time-mean water velocity field is presumed to be symmetric about the central vertical symmetry plane of the turbine. To reduce the computation effort required for convergence, it was presumed that the instantaneous water velocity field is also symmetric, thereby allowing the use of a vertical central symmetry plane and reducing the calculation domain volume by half. A schematic of this simplified calculation domain is shown in Fig. 3.

As can be seen in Fig. 3, the central floating body (hull) is absent from the domain. This is justified by the following two reasons: i) the exact shape of the hull was not fully defined during the preliminary design phase and ii) the project team was confident that the shape of the hull could be designed such as to augment the energy extraction of the screws (via local flow acceleration effects analogous to augmentation strategies). Subsequently, it was deemed preferable not to include the hull shape, as it resulted in conservative predictions which are desirable in a design exercise.

All main simulations were performed at the design free stream velocity ($V_{\infty,\,design}$) of 4 m/s, which is believed to be representative of the upper value range prevailing in the target prototype implementation site: the Bay of Fundy, located in Canada. Also, the turbine is presumed to be installed in sufficiently deep waters to consider the upstream water velocity magnitude constant with respect to the vertical direction over the full depth of the calculation domain. Impact of upstream flow non-uniformity is expected to be studied in upcoming design stages if implementation locations justify it.

As shown in Fig. 1 and Fig. 2, the JH turbine can operate when subjected to water currents aligned with is central hull axis, regardless of their direction. This means that it could remain essentially stationary in tidal applications and would not require yaw corrections. In the preliminary design phase and simulations, it was decided to focus on operation for a single water current direction, that is when water arrives from the apex formed by the extension of the V-shaped screw axes pair, as shown in Fig. 3. This is akin to considering a river application in which current direction would not alternate. Power production under reversed flow direction is expected to be similar in magnitude (for corresponding water free stream velocities), but not strictly equal. This will be investigated in upcoming design phases.

Lastly, it is assumed that the screw rotational speed is constant for a given studied case and that minute fluctuations about the time-mean value can be neglected. Indeed, due to the finite nature of the screw (presence of membrane start and end), the net torque produced by passage of the water flow is not strictly constant over a rotation cycle. It is presumed that the screw rotational inertia and the aforementioned generator regulation would minimize any fluctuation of the rotational speed.

B. Overall modeling approach

The CFD model was implemented in Siemens PLM Software STAR-CCM+ V13.02, a 3D finite-volume method (FVM) commercial package. This code was used in this case to solve the governing equations, namely the continuity, momentum (3D) and transported turbulence variables.

As can be expected, the water flow in the vicinity of the screws and in their wakes is turbulent. Consequently, turbulence was modeled using a Reynolds-averaged Navier-Stokes (RANS) turbulence model. It was decided to use the k-ω SST (shear-stress transport) proposed by Menter [13], mainly for its reputed accurate predictions of separation-prone flows. For details on the resulting set of governing equations, their precise implementation and numerical treatment, the reader is referred to [14]. These details are not reproduced here for conciseness reasons. The so-called "all y+ wall treatment" was used. This hybrid wall treatment: i) allows for a full resolution of the boundary layer if the near-wall mesh is sufficiently fine ($y+_{\text{cell centroid}} \sim 1$), ii) reverts to conventional wall functions elsewhere and iii) uses a blending function to bridge between treatments where required. Wall y+ values were monitored to ensure compliance with wall function limits, as these were employed by the aforementioned hybrid treatment over most the wall (screw) surfaces.

Second-order accurate discretization schemes were used to solve all dependent variables. The segregated-flow (non-coupled) solving strategy was employed.

As mentioned previously, focus was put on model cost-effectiveness, given the industrial context and time constraints (4 weeks). As of such, the original intent was to use a multiple reference frames (MRF, or "frozen rotor") approach, which would in turn allow for steady-state simulations. A cylindrical sub-domain volume

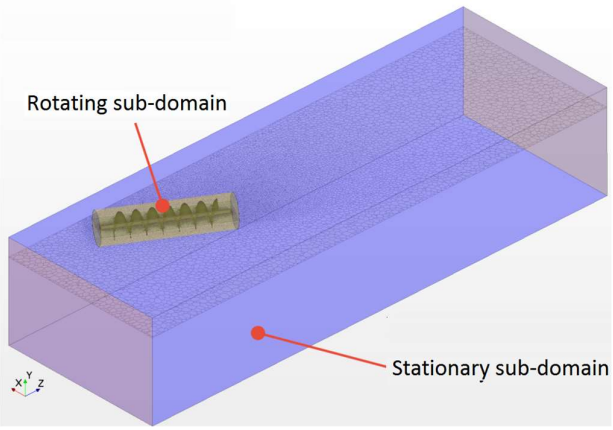

Fig. 4. Calculation domain comprising a rotating sub-domain (yellow) and a stationary sub-domain. Mesh plotted over horizontal plane coinciding with screw rotation axis, for visualization purposes. Air layer above water volume not shown.

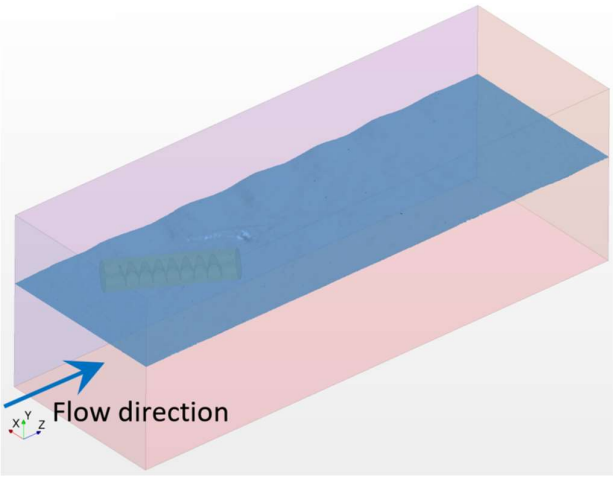

Fig. 5. Calculation domain used for free surface VOF model shown. The predicted water surface is shown for a typical time-step.

encompassing the rotating screw was defined while allowing sufficient distance with the screw edges. Preliminary simulations performed with this approach yielded physically implausible results and greatly underpredicted the energy-generation performance with respect to available test data. Additional trials were made by modifying the distance between the rotating cylindrical sub-domain interface and the screw edges. Numerical predictions remained essentially unchanged.

The poor performance of this modeling approach is explained next. Due to the oblique (non-parallel) angle between the screw axes and the incoming water flow, the actual flow field over the curved interface of the rotating cylindrical sub-domain is far from uniform in the local azimuthal direction (or along its circumference). This differs from cases in which the MRF approach is typically used, for example: stirring impellers in tanks or horizontal axis turbines facing the flow. In such cases, the fluid flow over the curved interface of the rotating sub-domain is typically tangential or normal to it and the velocity field remains relatively unchanged over the interface with respect to the azimuthal angle. The presence of a significant flow component incoming at an oblique angle with respect to the screw axes undermines the use of MRFs. Use of a so-called "mixing-plane" (circumferential spatial averaging) naturally did not alleviate observed inaccuracies.

Therefore, it was decided to use a "sliding" (rotating) mesh approach, which requires solving an unsteady problem. A rotating cylindrical sub-domain volume was generated around the screw. This sub-domain, and associated mesh, was rotated at each time-step, in accordance with the predefined screw rotational speed. A schematic of the resulting decomposed calculation domain is provided in Fig. 4.

Time marching was performed using an implicit, first-order accurate scheme. In a typical simulation, the screw rotational speed is prescribed and monitors, such as screw net torque, drag and lift, were surveyed until a time-periodic established regime was attained. Such a regime prevailed when the time-averaged values of the aforementioned monitors over the last rotational period differed by less than 1% from the previous one. This typically required about 15 to 20 rotational periods if the simulation were run from scratch. Fewer periods were required to reach an established regime if a simulation was initiated using the flow field of a case having a similar rotational speed. Lastly, a minimum of 5 iterations per time-step were performed for all simulations.

C. *Model cost-effectiveness considerations*

As mentioned earlier, efforts were made to implement an accurate, yet cost effective model which would yield predictions within a few hours. A simplification which was deemed worthwhile to investigate consisted of replacing the water free surface with a no-shear, no-normal flow boundary. This essentially allowed for a reduction of the computational efforts associated with the use of a free surface or volume-of-fluid (VOF) model.

Results yielded by a pair of simulations in which the no-shear surface approach and free surface VOF model were implemented were compared to verify the validity of this simplification. The calculation domain employed for the no-shear top surface case is shown in Fig. 4 whereas the one employed for the water free surface (VOF) model is depicted in Fig. 5. Except for the addition of an air layer above the water line, all other domain dimensions and solution parameters were kept identical (more details on domain sizing and boundary conditions are provided in the next subsection).

This set of simulations was solved using the initial screw design and for the following parameters: $V_\infty = 4$ m/s and $\omega = 6.283$ rad/s (60 RPM), resulting in a *TSR* value of 1.795. This value of ω was chosen as it corresponds to the optimal rotational speed of the original screw design which maximizes power generation performance.

The relative difference in predicted screw net torque and power coefficient between both simulations was less

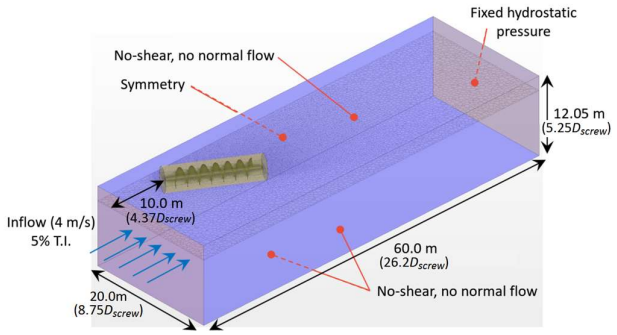

Fig. 6. Overall dimensions of calculation domain and boundary conditions. Mesh plotted over horizontal plane coinciding with screw rotation axis, for visualization purposes.

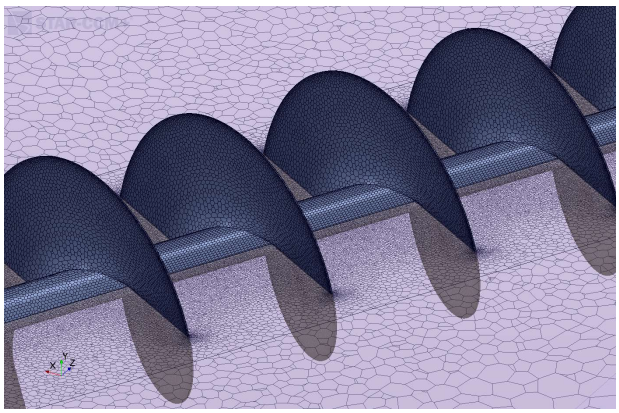

Fig. 7. Close-up view of the mesh near and over the screw surface (baseline mesh shown).

than 2.2%. Surprisingly, the free surface VOF simulation predicted a slightly superior power coefficient value with respect to the no-shear top surface case. This is counter-intuitive, since the no-shear top surface was expected to constrain the flow around the screw, thereby accelerating it and resulting in a superior torque and extracted power prediction. Nonetheless, this minimal difference in predicted power coefficients justified the use of the no-shear top surface approach. Also, visual inspection of the water surface predicted by the free surface VOF model indicates that the perturbation caused by the presence of the screws is barely perceptible (Fig. 5). This is corroborated by observations made during trials performed with the instrumented smaller scale test unit.

The resulting simplified CFD model still required substantial computing power and was solved using a power-on-demand cloud computing centre. Typically, 300 CPUs (E5-2680 v4 @ 2.40GHz) were used for most cases up whereas up to 1000 CPUs were required for mesh-size independence studies performed with the finest mesh. Real time required to reach the established time-periodic regime varied from about 2h for most cases up to 6h for mesh-size independence studies. These delays were deemed satisfactory by the project team and allowed for rapid interactions and iterations when needed. The model cost-effectiveness also resulted in a lower computing costs for the client, Jupiter Hydro.

D. Calculation Domain and Boundary conditions

The calculation domain overall dimensions are shown in Fig. 6, along with the boundary conditions. Dimensionless distances, normalized with the initial screw diameter D_{screw} as the reference length, are also provided. The dimensions of the rotating sub-domain, which is aligned and centred around the screw axis, are the following: diameter of 3.2 m (or 1.4D_{screw}) and length of 13.61 m (5.94D_{screw} or 1.06L_{shaft}).

As indicated previously, the incoming velocity is presumed to be constant over the corresponding surface (no dependence on depth) and the velocity magnitude was set equal to $V_{\infty,\,design}$ (4 m/s) in all cases. If the screw diameter is used to define a Reynolds number, this velocity results in $Re_{Dscrew} \approx 7.9\text{x}10^6$. The inlet turbulence intensity was prescribed as uniform and equal to 5%. The top, bottom and side boundaries were set as no-shear (no normal-gradient) and no-normal flow, which are analogous to symmetry in this case. Naturally, the remaining vertical surface corresponding to a symmetry plane was prescribed as such. At the outlet, a fixed hydrostatic pressure was prescribed. A no-slip condition was prescribed on all screw surfaces, which were presumed smooth for the sake of this exercise.

Prior to performing the mesh-size and time-step size independence studies, a sensitivity check on the domain size was performed to ensure that its limits were sufficiently distant from the energy extraction surfaces and allowed sufficient flow redevelopment length downstream of the wake to apply an outlet boundary condition. Doubling the domain dimensions in all directions resulted in a relative reduction of the predicted screw torque and power coefficient of 2.9% (at V_∞ = 4 m/s and ω = 6.283 rad/s or 60 RPM). This result is attributable to the relative blockage area of the screw being reduced as the domain size is increased, resulting in less induced acceleration of the flow around the screw. For cost-effectiveness reasons and considering the preliminary phase of the design, the domain dimensions shown in Fig. 6 were deemed sufficiently large.

E. Mesh-size and time-step size independence study

All meshes were generated within STAR-CCM+ using the polyhedral mesher. Prism layers, 5 control-volumes (CV) thick, were extruded over all solid (screw) surfaces. Additional mesh refinement was prescribed over the screw membrane surfaces and the membrane outer edge. A wake-type mesh refinement was also applied downstream of the screw and its rotating sub-domain. A close-up view of the resulting mesh (baseline) near and over the screw surface is shown in Fig. 7.

The mesh-size and time-step independence studies were conducted using the initial screw design and the following operating parameters: V_∞ = 4 m/s and ω = 6.283 rad/s or 60 RPM. Three meshes were generated for the purposes of the mesh-size independence study. Successive mesh refinement was applied by further

TABLE II
MESH CHARACTERISTICS AND RESULTS OF MESH-SIZE INDEPENDENCE STUDY

Mesh #	Number of CVs	Surface mesh size over screw membrane	Wall distance of first CV node over screw surface	Predicted C_P	Relative Difference
1	6 044 401	50 mm	0.47 mm	0.2985	- 5.2%
2	14 548 782	33.3 mm	0.32 mm	0.3044	- 3.3%
3	31 873 754	25 mm	0.24 mm	0.3150	0.0% (Ref.)

reducing the reference or base mesh size. All local mesh refinements were prescribed as a relative fraction of this base size, thus the local mesh size was progressively reduced throughout the domain in a proportional manner. The characteristics of all generated meshes are listed in Table II, along with the results of the study. The baseline mesh is identified as #1. The size refinement indices applied to meshes #2 and #3 (with respect to mesh #1) are 1.5 and 2, respectively. Surface mesh size values provided in Table II correspond to the prescribed edge length of the triangular elements initially generated over the screw membrane (later converted to polyhedral CVs), whereas the listed wall distances denote the distance between the node (centroid) of the wall-adjacent CV (within the prism layer) and the wall itself.

The mesh-size independence study simulations were performed using a time-step of 0.005 s. This resulted in 200 time-steps per screw rotation (at 60 RPM). The time-step size independence study, presented later in this subsection, demonstrated that this value was sufficiently small to consider the results as being essentially independent with respect to the time-step.

The discrepancies between C_P values yielded by the baseline (#1) and the finest (#3) meshes is 5.2%. Ideally, this discrepancy would have been inferior. Usage of mesh #2 or #3 for the main simulations and investigation of finer meshes would have been desirable, but prohibitive in terms of cost and project schedule. Given the preliminary stage of the design phase and these limitations, results yielded by mesh #1 were deemed satisfactory for the purposes of this study. Naturally, conducting a stricter mesh-size independence study, by using Richardson extrapolation and exploring finer (pattern-preserving) meshes, would be desirable in the upcoming project phases.

It is worth specifying that when the performance of modified (improved) screw designs was investigated in the course of the main study, refinements characteristics identical to those of mesh #1 were prescribed during the meshing procedure.

Lastly, a time-step size independence verification was performed. This was done by simulating the same case using mesh #1 and a time-step of 0.0025 s, a value equal to half that of the original baseline case. This translated into 400 time-steps per screw rotation (at 60 RPM). The key result, namely the predicted C_P value, increased by 1.1%. Consequently, results obtained with the baseline time-step were deemed sufficiently independent with respect to time-step size for the purposes of this study. Again, due to project time and cost constraints, investigation of finer time-step sizes at this preliminary design stage was not deemed necessary.

V. RESULTS AND DISCUSSION

The results of the main study are presented and discussed in the following subsections.

F. Model benchmarking with field measurements

The first step of the main study consisted of benchmarking the CFD model with field measurements performed by Jupiter Hydro. The measurements were provided in the form of power coefficient (C_P) values as functions of tip-speed ratio (TSR). These field measurements were obtained with an instrument test rig having screws of a diameter approximately half the size of those of the JH turbine (initial design) considered in this exercise. The test rig screws counted fewer membrane turns but had the same pitch as those of the full-scale turbine. The CFD model was adapted by incorporating these geometric details.

The CFD model was used to obtain multiple predictions of C_P over the range of TSR values investigated with the test rig (0.25 to 2.85). As can be expected for field tests performed under a lack of controlled conditions, significant scatter is present in the measurements. It is worth highlighting that similar experimental TSR values were attained via different combinations of free stream velocities and rotation speeds. Due to the important number of experimental points, the CFD model cases were solved using a constant

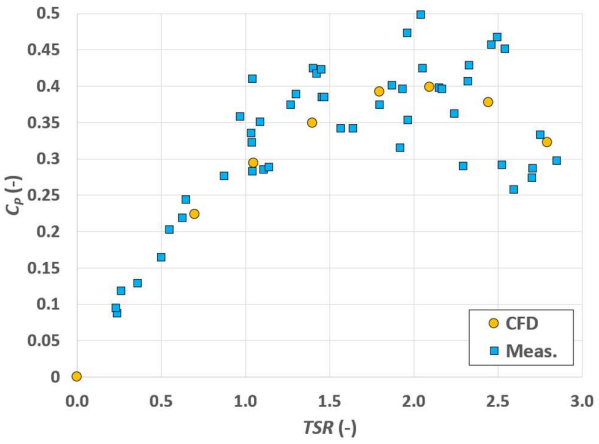

Fig. 8. Predicted and measured power coefficient values as a function of tip-speed ratio. Results of CFD model benchmarking simulations.

TABLE III
RESULTS OF JH TURBINE ENERGY-GENERATION MAXIMIZATION EXERCISE

Design #	$P_{max,mech}$ (kW, per screw)	TSR_{Pmax} (-)
1	126.9	1.80
2	149.7	2.10
3	167.5	2.10

free stream velocity matching the higher value prevailing during the experiments and by modifying the screw rotational speed solely.

The numerical predictions are compared to the field measurements in Fig. 8. The uncertainty of the measurements was not provided with the data and hence is not shown. The test rig was towed by a tug boat across a lake, thus the incident flow direction is believed to have been well controlled. The dominant uncertainties in measured C_P values are believed to stem from the rig velocity and torque measurements. These likely explain the relatively high (≈ 0.5) C_P values and the data scatter. Considering the latter and the lack of established models and methodology for modeling flows over these unconventional energy-extraction surfaces, the agreement between the numerical predictions and field measurements was deemed good. Therefore, it was decided to proceed with the proposed CFD model and perform the main simulations aimed at predicting and optimizing the energy-generation performance of the JH turbine.

Also, the impact of scale was briefly studied numerically by doubling both the rig screw size and free stream velocity, thereby multiplying the value of Re_{Dscrew} by 4. A relative C_P increase of 5.1% (at a *TSR* value of 2.1) was predicted for this higher Reynolds number case.

Prior to presenting the main results, it must also be added that directly comparing predicted C_P curves of screw geometries having different number of membrane turns can be misleading, as shorter screws with fewer turns tend to have higher C_P values. This is because the torque contribution of the upstream screw turns is superior to that of the downstream ones, which are subjected to a wake effect. Hence, a longer screw with more turns (and additional projected area, $A_{proj.}$) would generate more power while having a slightly inferior C_P value at corresponding *TSR*s.

G. *Screw design optimization and maximization of turbine energy-generation performance*

Following the benchmarking exercise, the CFD model was utilized to predict the performance of the JH turbine, starting from the proposed initial design. To generate at least 300 kW of electrical power at the design water free stream velocity, an extracted mechanical power of 165 kW per screw was chosen as the minimum allowable value by the project team. The first set of cases was aimed at investigating if the initial design met this performance criterion.

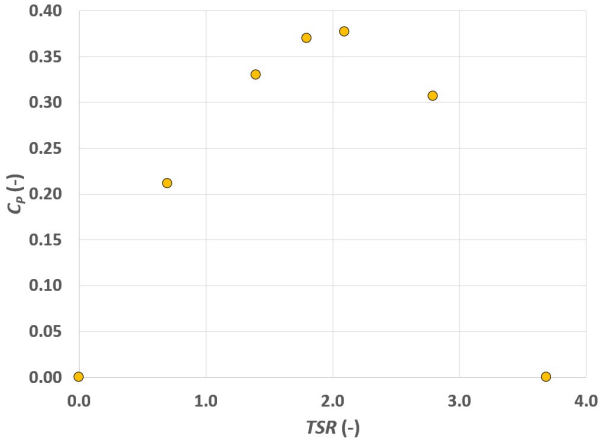

Fig. 9. Predicted power coefficient values as a function of tip-speed ratio for turbine design #3.

To this end, the CFD model was used to predict the power curve, namely the extracted mechanical power as a function of rotational speed, for the initial turbine and screw design. The maximum predicted mechanical power value, 126.9 kW, was attained at a *TSR* of 1.80. This performance was deemed insufficient and a design iteration was performed on the screw. A maximum mechanical power of 149.7 kW was predicted for the second design, which had a larger screw diameter, fewer membrane turns and the same $A_{proj.}$ value with respect to the first design. Consequently, a third screw design exercise, in which an additional membrane turn was added to the second design screw (hereby increasing $A_{proj.}$ without requiring an increase in shaft length L_{shaft}), was performed. The updated CFD model for this last design iteration predicted a maximum mechanical power of 167.5 kW. This was considered satisfactory by the team and further design iterations were not performed. The results of this energy-generation maximization exercise are listed in Table III in which maximum extracted mechanical power ($P_{max,mech}$) values are provided, along with the corresponding tip-speed ratio (TSR_{Pmax}).

The power curve predicted for the third screw design is illustrated in Fig. 9. Although no power can be produced when the rotational speed is null, this case was still solved for structural considerations and is thus shown in the figure.

The aspect of the power curve is the same as that shown earlier in Fig. 8. Extracted power is initially null at a *TSR* value of 0, it then increases progressively until the maximum values is attained (C_P = 0.377 at *TSR* = 2.10 in this case). After this point, the extracted power drops with increasing rotational speed until no net torque is produced (*TSR* = 3.69).

Interestingly, the maximum C_P value of the third design is inferior to that predicted for the test rig screws. This is mainly because the third screw design comprises more membrane turns than the rig test screw (see comments at end of subsection F). Naturally, the third screw design generates much more mechanical power due to its larger size and additional projected area ($A_{proj.}$).

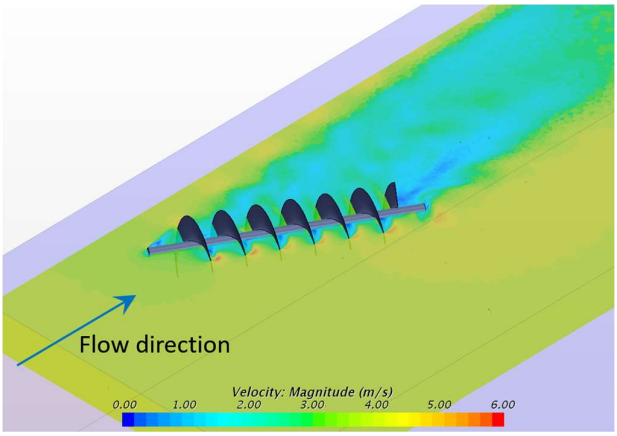

Fig. 10. Instantaneous velocity magnitude contour plot over horizontal plane coinciding with screw rotation axis. Velocity scale ranges from 0.0 to 6.0 m/s.

The predicted power curve for the final screw design would also allow the preliminary elaboration of the real-time regulation and control systems required to maintain the screw rotational speed at the optimal value during operation. Additional details on the flow patterns and mechanisms responsible for the generation of torque (and power) are provided in the next subsection.

Lastly, it is worth highlighting that the screw design optimization exercise was performed while respecting design constraints, such as allowable screw shaft length and diameter. Re-meshing the calculation domain between design iterations did not require more than one or two hours. Also, structural aspects had to be taken into account, even prior to initiating the FEA modeling exercise. As mentioned earlier, instantaneous static pressure fields prevailing over the screw surfaces were outputted at multiple instants over a screw rotation period. These pressure fields acted as boundary conditions in the FEA model used to validate the structural integrity of the screws.

H. Discussion on flow patterns and mechanisms responsible for torque and power production

The flow patterns and mechanisms responsible for the generation of a net torque on the screws are briefly discussed in this subsection. First, a contour plot showing the instantaneous magnitude of velocity over a horizontal plane coinciding with the screw rotation axis is shown in Fig. 10, for the following case: $V_\infty = 4$ m/s and $TSR = 2.1$.

The velocity deficit or wake is clearly visible downstream of the screw. Local flow acceleration around the screw edge can also be seen. As the flow approaches the upstream screw surface, it decelerates and gains static pressure. The flow separates over most of the screw edge and creates a low-pressure region behind the downstream surface of the membrane. This is illustrated in Fig. 11 where the instantaneous static pressure field (compensated for the hydrostatic effects) is plotted over the screw upstream and downstream surfaces at a given instant. This pressure difference across the membrane generates a net force in the direction normal to the surface. Since the membrane surface normal direction is not parallel with the screw axis, a torque is produced. Lastly, it is worth adding that numerical predictions indicate that the contribution of viscous shear stresses to the total net torque is minimal (< 5%) with respect to that of the pressure-induced forces.

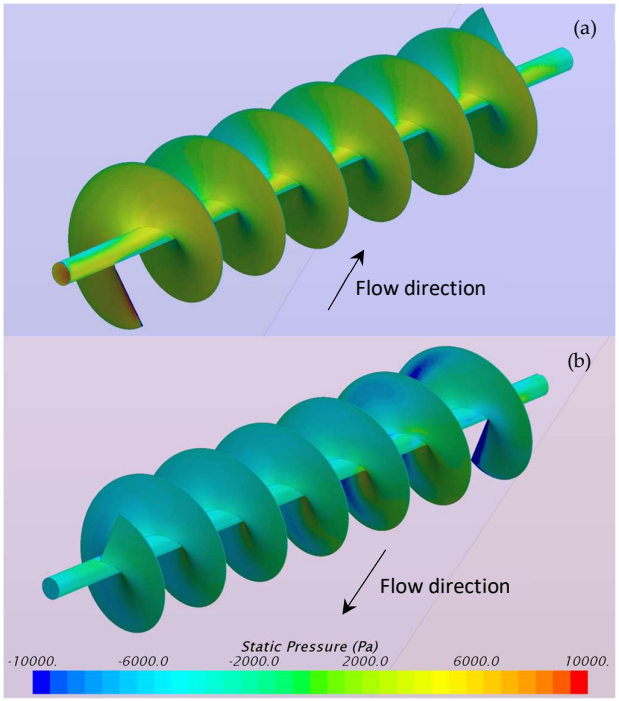

Fig. 11. Instantaneous static pressure (compensated) over screw (a) upstream and (b) downstream surfaces. Static pressure scale limited between -10000 Pa and 10000 Pa for visualization purposes.

VI. CONCLUSION

A cost-effective CFD model allowing for the prediction and optimization of the energy-generation performance of the JH turbine has been presented in this paper. The CFD model was successfully benchmarked against available field measurements. It was then used to predict the performance of the JH turbine and perform design iterations as needed to maximize extracted power and ultimately, meet the required energy-generation criterion. This exercise was performed under tight budgetary and time constraints (4 weeks).

Future modeling efforts in the upcoming design phases are expected to include: i) stricter mesh-size independence studies and use of finer meshes for the main simulations, ii) additional model validation with latest test rig or prototype field measurements, iii) addition of the central floating body (hull) in the calculation domain and use of the CFD model to optimize its shape and iv) study turbine stability aspects and mooring requirements by performing solid body motion simulations, if required.

REFERENCES

[1] M. J. Khan, G. Bhuyan, M. T. Iqbal and J. E. Quaicoe, "Hydrokinetic energy conversion systems and assessment of horizontal and vertical axis turbines for river and tidal

applications: A technology status review," *Applied Energy*, vol. 86, pp. 1823-1835, 2009.

[2] M. S. Güney and K. Kaygusuz, "Hydrokinetic energy conversion systems: A technology status review," *Renewable and Sustainable Energy Reviews*, vol. 14, pp. 2996-3004, 2010.

[3] M. I. Yuce and A. Muratoglu, "Hydrokinetic energy conversion systems: A technology status review," *Renewable and Sustainable Energy Reviews*, vol. 43, pp. 72-82, 2015.

[4] M. J. Khan, M. T. Iqbal and J. E. Quaicoe, "River current energy conversion systems: Progress, prospects and challenges," *Renewable and Sustainable Energy Reviews*, vol. 12, pp. 2177-2193, 2008.

[5] H. H. H. Aly and M. E. El-Hawary, "The current status of wind and tidal in-stream electric energy resources," *American Journal of Electrical Power and Energy Systems*, vol. 2, pp. 23-40, 2013.

[6] Canadian Hydraulics Centre, "Assessment of Canada's hydrokinetic power potential - Phase I report methodology and data review," March 2010.

[7] S. L. Ortega-Achury, W. H. McAnally, T. E. Davis and J. L. Martin, "Hydrokinetic power review," April 2nd 2010.

[8] J. VanZwieten, W. McAnally, J. Ahmad, T. Davis, J. Martin, M. Bevelhimer, A. Cribbs, R. Lippert, T. Hudon and M. Trudeau, "In-stream hydrokinetic power: Review and appraisal," *Journal of Energy Engineering*, vol. 141, 04014024, 2014.

[9] M. J. Lawson, Y. Li and D. C. Sale, "Development and verification of a computational fluid dynamics model of a horizontal-axis tidal current turbine," in *30th Int. Conf. on Ocean, Offshore, and Arctic Engineering*, Rotterdam, The Netherlands, 2011, pp. 1-10.

[10] T. J. Hall, "Numerical simulation of a cross flow marine hydrokinetic turbine," Master Thesis, Mech. Engineering, University of Washington, USA, 2012.

[11] P. Marsh, D. Ranmuthugala, I. Penesis and G. Thomas, "Three-dimensional numerical simulations of straight-bladed vertical axis tidal turbines investigating power output, torque ripple and mounting forces," *Renewable Energy*, vol. 83, pp. 67-77, 2015.

[12] V. S. Neary, A. A. Fontaine, P. Bachant, B. Gunawan, M. Wosnik, C. Michelen, R. J. Meyer and W. A. Straka, "US Department of Energy (DOE) National Lab activities in marine hydrokinetics: Scaled model testing of DOE reference turbines," in *European Wave and Tidal Energy Conf.*, Aalborg, Denmark, 2013.

[13] F.R. Menter, "Two-equation eddy-viscosity turbulence modeling for engineering applications," *AIAA Journal*, vol. 32, pp. 1598-1605, 1994.

[14] Siemens PLM Software, "Theory guide", V13.02, 2018.